Hall Effect Sensor-Based Low-Cost Flow Monitoring Device: Design and Validation

Margit Egerer, Asko Ristolainen, Laura Piho, Lauri Vihman, and Maarja Kruusmaa

***Abstract*—Monitoring and assessment of coastal and river velocities plays a key role in both scientific and industry applications. Field measurements are key for decision-making for resource management and protection, as well as for the validation of numerical models and climate change studies. In this article, a Hall effect sensor-based cost-effective novel device is proposed for measuring velocities and direction of near-bed currents and water-level. This device, called the Hydromast, provides instantaneous measurements in real-world conditions and is equipped with communication capabilities to allow near real-time data transfer and monitoring. The validation of the device is performed in real-world steady and unsteady flow conditions. Within the device measurement range, it is shown that the root-mean-square error (RMSE) of the time-averaged flow measurements is under 0.1 m/s.**

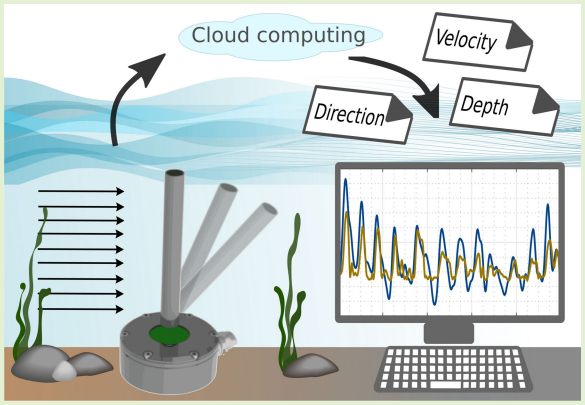

***Index Terms*— Flow direction, flow velocity, near-bed measurements, remote data transmission, water current measurements.**

I. Introduction

MEASURING flow velocity in the field conditions plays a significant role in many scientific and industry applications, for example, in hydrological studies [1], sediment transport investigations [3], [4], [5], the determination of aquatic habitats [6], [7] in rivers, estuaries, and coastal waters, and flood warning systems [8]. Near-bed velocity estimates are key metrics in sediment transport and river habitat studies [9], [10].

Popular in situ field measurement devices for flow velocity are propeller velocity flowmeters, acoustic Doppler velocimeters (ADVs), and acoustic Doppler current profilers (ADCPs). In addition, there have been efforts to develop remote-sensing methods, from the use of radars for estimating surface velocities to satellite imagery for river discharge estimation [11], [12]. However, the aforementioned methods have either good temporal resolution or good spatial resolution, not both. The acoustic measuring devices (ADV and ADCP) have a good temporal resolution of 50 Hz, whereas the spatial resolution depends on the number of devices. Due to the high cost, in general, not many of these devices are used together, especially over long periods of time and in extreme environments where the chances of recovering the instruments go down. Satellite models, for example, Planet Labs satelite SkySat [13], [14], have good spatial resolution (about 0.5 m). However, the temporal resolution of SkySat is 4–5 days [13], [14].

Further problems can arise when measuring near-seabed or near-surface velocity, as local wake features can affect the measurements near the bed and air entertainment, secondary currents, and velocity tip effect can influence near-surface measurements [15]. In addition, remote-sensing methods are restricted to estimating water surface velocity [16], [17], [18]. In [19], it is shown that to obtain reliable average velocities in a flow affected by natural turbulence and instrument noise, a sampling duration of 90 and 150 s is found to be sufficient for ADV and ADCP, respectively. For long-term behavior and large-scale spectral analysis, when many sources of flow variability are present, a longer sampling duration is needed. This means that for reliable estimation of near-surface velocities, ADV and ADCP temporal resolution also decreases.

Despite the challenges, for many applications, continuous instantaneous flow measurements are extremely important.

Manuscript received 31 August 2023; revised 24 November 2023; accepted 3 January 2024. Date of publication 22 January 2024; date of current version 29 February 2024. This work was supported in part by the European Union through European Social Fund Project "ICT Programme," H2020 Project ILIAD under Grant 101037643, in part by the H2020 Project LAKHSMI under Grant 635568; and in part by the Estonian Research Council funded Project SolidShore under Grant EMP480. The associate editor coordinating the review of this article and approving it for publication was Prof. Sheng-Shian Li. *(Corresponding author: Margit Egerer.)*

The authors are with the Centre of Biorobotics, Department of Computer Systems, School of Information Technologies, Tallinn University of Technology, 12618 Tallinn, Estonia (e-mail: margit.egerer@taltech.ee).

Digital Object Identifier 10.1109/JSEN.2024.3354194

Sediment motion depends on momentary flow features [20], flow type characterization [21], and feature detection in flows (e.g., ship detection [22]) and requires high temporal resolution, studying stresses on submerged structural elements benefit from long-term continuous monitoring [23]. Therefore, there is a need for cost-effective methods to provide continuous, reliable, and distributed data on the near-bed velocities.

Motivated by the changing hydrological conditions imposed by the climate crisis and the need for near-bed continuous measurements, a method for in situ observations of flow velocity was proposed by Ristolainen et al. [24]. A bimodal flow sensing device using accelerometers was designed and used to automatically classify river hydromorphology [25], and new methods for near-bed velocity measurement were developed [26]. Unfortunately, this device, the original Hydromast, had several drawbacks: it had a limited flow velocity range, it could only estimate the average mean flow velocity, and it was not capable of real-time data output. The lower end of the measurement range was too high for many near-bed applications, allowing only measurements in constantly fast flows. Additionally, no measurements were possible in wave-driven coastal applications, with regularly changing flow direction and only local storage was possible, allowing data processing and output only after the recovery of the devices.

To address the described limitations, a novel design of the Hydromast based on a Hall effect sensor has been proposed and a cloud-based communication setup has been designed, granting near real-time (latency couple of seconds) data transfer and observations by the user. The upgraded device, from now on referred to as the Hydromast, uses magnetic field sensing at the base to instantaneously detect the exact tilt and direction of the sensing element. This allows simpler and faster estimation of flow velocity and additionally allows us to measure the direction of the flow. Changing the length of the sensing element allows for varying the velocity measurement range according to the application. Moreover, the new design allows for instantaneous flow estimates and opens up a new application range of unsteady flow measurements in rapidly changing environments. The device has been validated in various flow fields together with a baseline measurement for determining the behavior, robustness, and durability in real-life environments and demonstrating possible applications. This leads to an accurate, robust, and cost-efficient way to measure continuous near-bed current velocity.

The organization of this work is as follows. Section II introduces the working principle, device design, and upgrades. Section III describes the calibration methods and results. Section IV provides the description and results of the field validations in both steady and unsteady flows. Sections V and VI discuss the results and performance of the device presented in the article and bring out the potential applications, strengths, and weaknesses of continuous instantaneous velocity estimation with the Hydromast.

II. Hydromast Design and Working Principle

The Hydromast is inspired by the neuromast, which is the major unit of functionality of the biological lateral line. A neuromast, being a mechanoreceptive organ of fish, is responsible for the sensing of mechanical changes in the surrounding flow field [2]. The Hydromast consists of a rigid mast that is fixed to the base with a flexible membrane, resembling an upscaled version of a neuromast. The bulk flow velocity over the mast generates vortex-induced vibrations (VIVs) of the mast which dominate over the random forcing due to turbulent flow conditions.

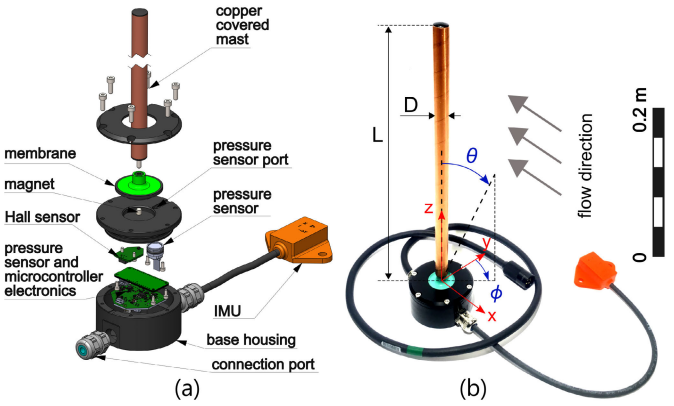

Fig. 1. Hydromast overview. (a) Hydromast exploded view. (b) Assembled hydromast with axes x, y, and z, mast tilt angle θ and direction ϕ, as well as mast length L and diameter D.

A. Hydromast Design

In the previous Hydromast designs by [24] and [26], the mast motion was recorded with a micromechanical inertial measuring unit (IMU). Our upgraded Hydromast design uses a 3-D Hall effect sensor (TLV493D-A1B6, Infineon Technologies AG) to track the mast movement. The Hall effect sensor, located in the Hydromast base, detects the strength of the magnetic field from a 5 × 5 mm neodymium cylindrical magnet installed at the base of the mast inside the flexible membrane. A main benefit of implementing magnetic field sensing is the instantaneous position estimation of the mast for instantaneous tilt angle and direction measurements. Also, the contactless sensing of magnetic fields improves the robustness of the device, as no cables are connected to and affect the vibrating mast. This also simplifies and reduces the cost of manufacturing. Similar to the previous design, the Hydromast can be equipped with an external IMU (MinIMU-9, Pololu Corporation) to detect the installation angle and device base movements in unsupervised installations onto sea bead.

The device consists of a CNC-machined polyoxymethylene (POM) base, a flexible membrane, and a mast. The mast is a hollow polycarbonate (PC) tube, closed at both ends and mounted to a flexible silicon membrane (Elite Double 22, Zhermak SpA). The mast has air inside that makes it positively buoyant and a higher natural frequency f_N compared to the water-filled mast. An air-filled mast is more sensitive to the flow and is therefore the preferred setup, as described later. The mast is covered with a 0.06 mm thin layer of copper to minimize biofouling during longer deployment periods. The standard diameter of the mast used in this work is $D = 15$ mm, but the dimensions can easily be altered for specific applications. The length of the mast L can be varied depending on the needed measurement range.

The base housing incorporates PCBs of the microcontroller (Adafruit Feather with Atmel ATSAMD21 Cortex M0 processor), power, serial communication, and pressure sensor. An absolute pressure sensor records the water height (86-030A-R, TE Connectivity) with the pressure port integrated into the POM casing (with a range of 0–2 bar). The Hydromast can be connected directly over an RS485 serial connection to a PC or to a communication module with a raw data sampling rate of 50 Hz. The Hydromast power consumption is approximately 0.15 W (at 5 V supply voltage). The cost of the Hydromast components is about 500€ at the time of writing this article. The design of the Hydromast is shown in Fig. 1(a).

B. Working Principle

The Hydromast measures the mast location in the x-, y-, and z-direction using magnetic field, with Hall sensor outputs X, Y, and Z (in mT) accordingly. The coordinate system of the mast is shown in Fig. 1(b). The magnitude

$$M_{XYZ} = \sqrt{X^2 + Y^2 + Z^2} \tag{1}$$

reading is observed to be linearly correlated to the tilt angle θ of the device, whereas the components X and Y correlate to the mast location in the xy-plane and indicate the direction of the flow, noted as $\bar{\phi}$. Two different methods of flow velocity estimation can be introduced: 1) velocity estimate V_f based on the dominant frequencies f_d of the mast vibration (time-averaged estimate) and 2) velocity estimate V_θ based on the tilt θ of the mast (instantaneous estimate).

Fluid-body forces govern the interactions between the mast due to VIV. Each Hydromast has its own natural frequency f_N that is the frequency the mast oscillates with when disturbed and no forcing (i.e., flow) is present. When a cylindrical rod is put in a cross-flow, it generates vortices with a vortex shedding frequency f_0. The first velocity estimation method of the Hydromast is based on the vibrations of the elastically supported rigid mast as a VIV resonator. In [24], the design of the device was tuned so that the lightly damped cylinder would oscillate with frequency f as close as possible to the vortex shedding frequency f_0. It was shown that the time-averaged velocity can be estimated using the mean frequency spectral amplitude after taking the fast Fourier transform (FFT) of the mast vibrations (for more details refer to [26]). When the cylinder vortex shedding frequency is close to the natural frequency $f_0 \approx f_N$, an important lock-in phenomenon occurs: $f_0/f_N = 1$. In such cases, the shedding becomes controlled by the natural frequency, even if small fluctuations in the flow velocity occur. This and other resonance points of a lightly damped cylinder are related to the bulk flow by reduced velocity $V_r = V/(f_N D)$, where V is the velocity of the bulk flow and D the diameter of the cylinder [27]. For frequency-based velocity estimate V_f, a relation based on the Strouhal number can be introduced, $St = f_0 D/V$. For the Hydromast, the relation between dominant frequency $f_d(M_{XYZ})$ and flow speed can be written as follows:

$$V_f = \frac{D}{St} f_d + C_0 \tag{2}$$

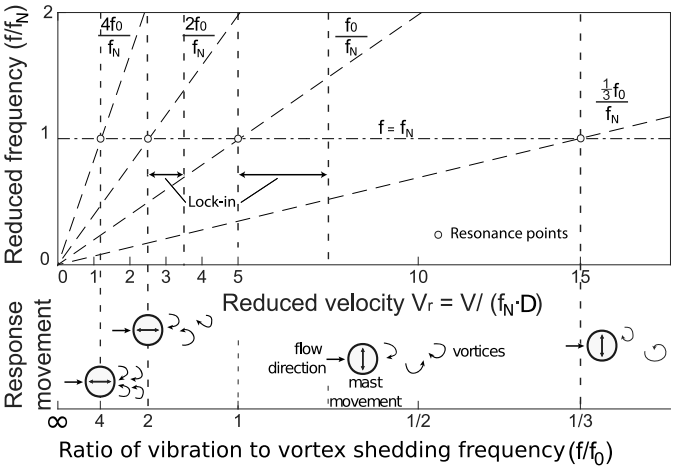

Fig. 2. Schematic response of lightly damped cylinder in crossflow (adapted from [27]).

where C_0 is a constant taking into account the end-effects (of the mast tip) and other artifacts of the specific device setup. For a stationary smooth circular cylinder for Reynolds numbers ranging from 10^3 to 10^5, the Strouhal number of vortex shedding is $St \approx 0.2$ [28]. Using $St = 0.2$ reduces (2) to $V_f = (D/0.2) f_d + C_0$, where only C_0 needs to be empirically determined.

In [26], a 100-mm-long neutrally buoyant mast was used, which provided a working range from 0.5 to 1.4 m/s. One of the goals of this study was to extend the working range of the Hydromast, especially to decrease the lower limit. This is done by choosing the mast with a correct natural frequency, based on the needed measurement range. Response to the cross-flow of a lightly damped circular cylinder is thoroughly described in [27]. If a cylinder is free to vibrate in any direction perpendicular to its axis, many modes of vortex shedding can occur. The most important excitation occurs from resonance when vibration frequency f becomes equal to natural vortex frequency f_N, where the vibration amplitude drastically increases and lock-in at the high amplitude vibrations is observed. This response mode starts around $f/f_N \approx 1$ and can at most last down to $f/f_N = 1/3$, in the range of reduced velocity of $5 < V_r < 15$, as schematically shown in Fig. 2. This is also the range where the Hydromast vibrations occur and flow velocity can thus be determined, defining the measurement range for the Hydromast. Minimum and maximum velocities are found as follows:

$$V_f \min = 5 D f_N \tag{3}$$

and

$$V_f \max = 15 D f_N \tag{4}$$

where f_N is the natural frequency in water.

For the second velocity estimate, V_θ, the exact position of the mast in time is determined using the Hall effect sensor outputs. This allows measuring tilt angle θ, nearly instantaneous flow speed V_θ as a function of θ, and flow direction $\bar{\phi}$. The tilt angle is assumed to be in a linear correlation with the Hall sensor measurements and can be calculated as

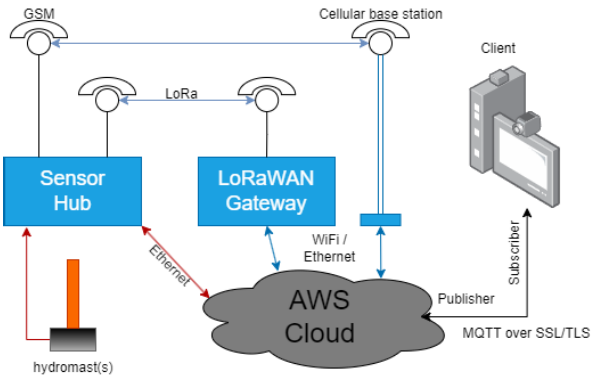

Fig. 3. Communication framework overview.

$\theta = p_1 M_{XYZ} + p_2$, where p_1 and p_2 are empirically detected calibration constants.

Mast tilt angle θ is linearly dependent on the magnitude of the magnetic field and therefore velocity can simply be correlated to M_{XYZ} as follows:

$$V_\theta = C_1 M_{XYZ} + C_2 \tag{5}$$

where constants C_1 and C_2 are found through calibration. Magnitude itself is used here, instead of θ to avoid introducing unnecessary extra uncertainty, as θ itself is also determined using calibration fit. It is important to note that this instantaneous velocity measurement based on mast tilt V_θ is independent of the frequency-based measurement V_f and can, therefore, be used as a separate measurement quantity.

The flow direction $\bar{\phi}$ can be found directly using Hall effect sensor outputs X and Y as instantaneous mast direction $\phi = \text{atan2}(X, -Y)$ which represents the mast location. To find the flow direction, an average over several vibrations must be calculated, taking the median value over some time, denoted with $\bar{\phi}$.

In addition to flow measurements, the Hydromast can also be used to measure the water level changes. The device is equipped with a pressure sensor enabling continuous measurement of the water level above.

C. Communications

In addition to modifying the sensing methods and hardware, the Hydromast now incorporates communication capabilities, enabling near real-time flow monitoring and device failure detection [30], [31]. These enhancements have expanded the range of potential applications for the device. To achieve this, a sensor hub based on Raspberry Pi 3 is utilized (we have also tested Beaglebone, and it is possible to use another ARM-based single-board computer). Fig. 3 shows the overview of the communication framework. The sensor hub stores data locally and transmits it to Amazon Cloud IoT Core using the MQTT protocol. In addition, the sensor hub can receive configuration updates from MQTT, specifically the connected mast types and calibration constants (see Section III). Infrastructure as code (IaC), specifically AWS cloud development kit (CDK), is employed for configuring and managing AWS services, which allows consistent configurations and stronger security. The source code for both self-developed components and IaC is maintained in GIT repositories. Python 3.9 and ReactJS are used for programming the self-developed components, including the web interface.

The sensor hubs operate on self-developed applications in a Docker container running on BalenaOS, and their management is facilitated through BalenaCloud servers. For communication with the Amazon Cloud, various options are available, including the use of a GSM network, LoRaWAN radio connection, and Ethernet communication. The proposed networking framework makes the Hydromast deployment both secure and scalable but also efficiently manageable from the sensors fleet's point of view.

III. Calibration and Characterization

To demonstrate the behavior and characteristics of the device, characterization was first performed in the lab, after which the field tests were done to calibrate the device.

A. Natural Frequencies and Measurement Range

For simple measurement range estimation, the mast's natural frequency dependence on the length was characterized. Natural frequencies in water and air for masts with varying lengths and mass were measured. The relation between L and f_N in water was represented by a power fit $f_N \sim L^a$, where a is a constant, whereas the ratio of natural frequencies was found to be $f_{N\text{air}}/f_{N\text{water}} \approx 1.4$. The natural frequencies and corresponding sensor measurement limits V_f min and V_f max are shown in Table I. Using these estimated ranges, the mast length can be chosen based on the measurement range needed in each specific application. For an extended measurement range, a setup with multiple Hydromasts can also be used, so that depending on the flow velocity, data from the correct device is acquired. It was chosen to continue with a positively buoyant mast due to its higher natural frequencies and faster response to the flow changes, to better capture unsteady flow phenomena. It must be noted that the tension restraint force to counteract buoyancy is larger for longer masts (due to larger volume) which can also change the performance characteristics.

For validation purposes, two masts were chosen: HM300 with $L = 300$ mm and HM200 with $L = 200$ mm length, both highlighted in Table I. These two masts together cover a range from $V = 0.1$ to 0.7 m/s being sufficient for many applications and they also have a wide enough range overlap to make comparisons.

B. Tilt Angle Calibration

The tilt angle θ was expected to be linearly correlated to the Hall sensor's output magnitude M_{XYZ}. A table-top calibration was performed, to determine the calibration coefficients. The mast was tilted at 11 different angles from $0° < \theta < 30°$ in eight different directions with 45° increments. The mast tilt was recorded using a Go-Pro camera and the tilt angle was calculated from the image. The angle showed a very good linear correlation with the output magnitude M_{XYZ}, as shown in Fig. 4. The calibration constants were found to be $p_1 = 1.2$ and $p_2 = 1.13$, with a coefficient of determination R^2 of 0.98.

TABLE I
CHARACTERISTICS OF HYDROMASTS BASED ON MAST LENGTH

Mast	L [mm]	mass m [g]	Buoyancy	f_N water [Hz]	f_N air [Hz]	$V_f min$ [m/s]	$V_f max$ [m/s]
HM50	50	9.4	positive	17.3	25.0	1.30	3.90
HM100	100	13.1	positive	7.5	12.2	0.56	1.69
HM100NB[1]	100	20.6	neutral	6.9	9.1	0.52	1.55
HM150	150	21.9	positive	4.9	6.5	0.37	1.10
HM150NB[1]	150	30.3	neutral	3.7	5.0	0.27	0.82
HM200	200	27.5	positive	3.1	4.2	0.23	0.69
HM300	300	39.4	positive	1.7	2.2	0.13	0.39

[1] NB - neutrally buoyant mast

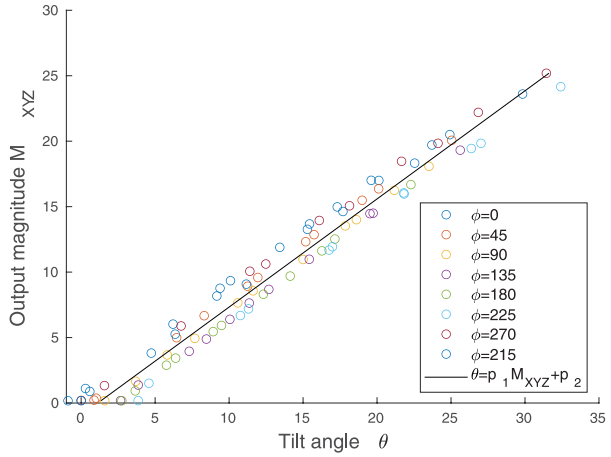

Fig. 4. Hydromast tilt angle calibration. Output magnitude M_{XYZ} for varying tilt angle θ with the linear fit. Measurements shown for eight different directions from $\phi = 0$ to $\phi = 315$.

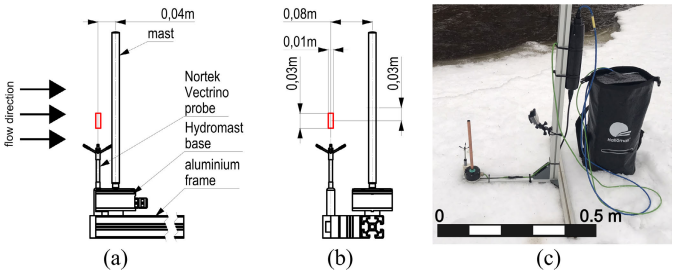

Fig. 5. Setup for the in-flow velocity calibration in a river. (a) Side view and (b) front view with the ADV and Hydromast (HM300) placement. (c) Assembled setup in the field.

C. In-Flow Velocity Calibration

The Hydromast velocity calibrations need to be determined in real flow conditions, where the turbulence levels, velocity profile, and setup are similar to the planned field applications. The Hydromasts were first tested in a small lab-scale flow channel. However, as the channel was too small for these devices and flow conditions were significantly different from real flow, this proved to be too unreliable and inaccurate for calibration purposes. Therefore, all calibration characterization was performed in a natural river flow.

The calibrations for flow velocity were conducted in Keila River (latitude 59.394537 N, longitude 24.294915 E; closest address Posti 1, Keila-Joa, 76 701 Harjumaa, Estonia) with the average water level of 102 cm measured at Keila river hydrological station [32]. The aim was to calibrate the Hydromast against ADV measurements (Vectrino Profiler, Nortek, Norway) in real-world conditions. ADV was chosen as a reference because it is a commercially available standard device for this type of flow measurement. An overview of the calibration setup is shown in Fig. 5. One Hydromast was deployed together with an ADV for reference measurements. Samples with a duration of 60 s were taken at 47 locations for HM300 and 29 locations for HM200. The Hydromast and ADV measurements were synchronized by using the sync signal from the ADV to trigger the recording of the Hydromast data logger (based on a Raspberry Pi 3, Raspberry Pi Foundation in association with Broadcom).

For all calibration and steady flow experiments, the Hydromast data acquisition rate was 50 Hz. When calculating V_f, no preprocessing of the data was done, the average velocity estimate was based on the frequency spectrum of the raw data throughout the sample. For calibration, 60 s long samples were first recorded and by looking at the convergence, it was determined that at least a 20 s sample is needed for an accurate dominant frequency estimate. Based on this, the calibration and validation sample length was chosen to be 30 s. Similarly, the tilt-based velocity estimates, V_θ, were first done based on raw data. As the interest lay in the time-averaged velocities, an average V_θ was calculated throughout the sample using $\tilde{V}_\theta = \text{median}(V_\theta)$.

In the calibration as well as steady flow validation experiments, the ADV data acquisition rate was 25 Hz and the ADV data processing was kept minimal. All steady flow experiments were done in real conditions and close to the surface. Hence, to reduce the noise in the averages due to different natural and device-caused phenomena (more details about ADV noise sources can be found in [29]), the median ADV velocity was also calculated throughout the 30 s sample.

Fig. 6(a) shows the calibration data for HM300 and HM200 together with the calibration curves for the dominant frequency-based velocity estimate V_f. It can be seen that a linear fit with constant slope D/St and calibration constant C_0 is a good approximation and describes well the relation between flow velocity and mast vibration, with $R^2 = 0.87$ for HM300 and $R^2 = 0.96$ for HM200. For calibration, all data was used, where a clear energy peak in the frequency spectrum could be determined. For HM300, peaks were detected for velocities from 0.15 to 0.50 m/s, and for HM200 the range was from 0.27 to 0.70 m/s. These ranges agree well with the theoretical estimates from Table I, according to which HM300 should work from 0.13 to 0.39 m/s and HM200 from 0.23 to 0.69 m/s. These calibration results agree well with the analysis described in Section II-B and support the theoretical assumptions. This calibration shows that dominant frequency

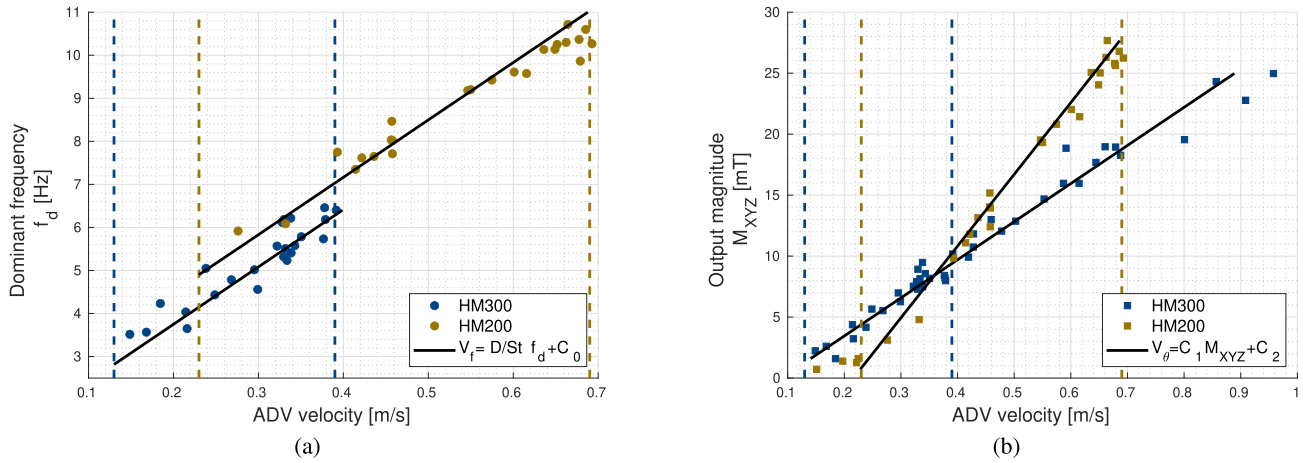

Fig. 6. Velocity calibrations of 200- and 300-mm masts. (a) Dominant frequency-based velocity V_f calibration. (b) Tilt-based velocity V_θ calibration. Calibration fit shown as a solid line, theoretical velocity limits $V_f$min and $V_f$max are shown as a dotted line.

can be used for flow velocity estimation and also, if needed, several devices with different ranges can be used to extend the measurement range.

Another method of determining velocity is using the tilt angle θ. Calibration data and linear fits for this method with both Hydromasts are shown in Fig. 6(b). Here, all calibration points are shown (averaged over 30 s) and it can be seen that both HM300 and HM200 have a linear dependence on the magnitude M_{XYZ}, with $R^2 = 0.96$ for HM300 and $R^2 = 0.96$ for HM200. The lowest speeds, at which the velocity can be measured, are 0.15 and 0.22 m/s for HM300 and HM200, respectively, being similar to the lowest limit where V_f can be used. HM200 has a higher slope, making it more sensitive to velocity changes, whereas HM300 has a slightly lower sensitivity. The tension restraint force to counteract buoyancy is almost double for the HM300 mast compared to HM200 and this seems to make the longer mast HM300 less sensitive to tilt due to flow velocity. This lower sensitivity constitutes a close to five times bigger measurement range for the HM300, with a new range spanning from 0.15 m/s up to nearly 1 m/s. This is a large increase in the range of the velocity measurement for HM300 compared to the working range for V_f (which was up to 0.39 m/s), expanding the applicability of the Hydromast significantly. Hence, the tilt provides an accurate estimate of flow velocity with the extra benefit of having a wider measurement range compared to the frequency-based estimate for HM300. It must be noted that the membrane of each Hydromast is currently hand-made and, therefore, the tilt calibration can also be slightly affected by the membrane properties. Therefore, sometimes, it can be useful to check with V_f the validity of the V_θ calibration if devices with new membranes are used.

To have independent measurements with the Hydromast, it is important for the device to detect when the measurements are in the working range and recognize and remove outputs when the Hydromast is out of range providing unreliable data. For V_f, this "out-of-range" criterion is defined by setting a minimum limit for spectral amplitude level at a dominant frequency so that only distinct high energy peaks are detected. For the Hydromast analysis, two dominant frequency peaks are detected in the spectrum (due to the eight-shaped movement of the mast) and the second one, at a higher frequency, representing the cross-flow vibrations, is chosen to be the estimate. This criterion depends on the length of the Hydromast and is determined based on the calibration data. For tilt angle-based estimate V_θ the "out-of-range" criterion is simply the minimum and maximum values for the magnitude M_{XYZ}, also determined based on the calibration results.

IV. Validation

The validation of the Hydromast velocity estimations was performed in three stages. First, validation was performed in steady flow conditions in a river, with many 30 s measurements. In the second stage, two devices were installed for a long period in steady flow in a river, to show long-term data and validate communication capabilities. This flow is steady in the short term but has variations over a longer time. Finally, the validation was performed in unsteady flow conditions on the coastline to demonstrate and validate the capability of the Hydromast to measure unsteady flows.

A. Steady Flow, Short-Term Tests

The short-term validation tests were performed on the same site as used for calibration but at different flow conditions. Measurements were taken in many locations in the river to show the performance of the device with the same setup at many different flow speeds. Measurement points were chosen to take into account the working ranges of the Hydromasts and steady flow conditions.

A setup with two Hydromasts, HM300 and HM200, together with the ADV (Vectrino Profiler) was assembled as shown in Fig. 7. The validation was performed in Keila River on the same location as the calibration experiments described in Section III, with a higher water level (water level of 112 cm measured at Keila water level station [32]) which allowed finding locations with a wide range of flow velocities. A total of 139 samples were collected over a range of velocities from 0.01 to 1.05 m/s.

The results of the velocity estimations based on the mast vibrations are shown in Fig. 8(a) and (b) for HM300 and

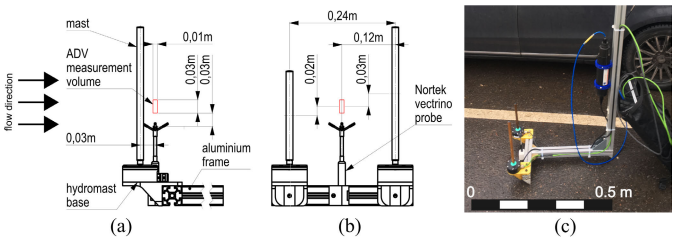

Fig. 7. Setup for steady flow validation tests in a river. (a) Side view and (b) front view with the ADV and Hydromast (HM300 and HM200) placement. (c) Assembled setup in the field.

HM200, respectively. ADV measurement serves as our reference velocity. It must be noted that also these measurements have uncertainty and to visualize that, the ADV measurements are shown with standard deviation (SD) (shaded in gray), which can be considered as the uncertainty of the reference measurement. Points, which according to ADV have high turbulence intensity (TI) levels, above 40%, are indicated with pink in the figures.

Comparison of V_f from the longer HM300 with ADV is shown in Fig. 8(a). Hydromast data agrees well with the reference ADV, having root-mean-square error (RMSE) of 0.065 m/s and all velocities detected lay within the estimated measurement range, between V_f min and V_f max, indicated as a shaded box in the figure. In this case, the majority of the data detected lies within the theoretical measurement range, supporting the theoretical model. The used criteria of minimum energy level at dominant frequency works well for peak detection, only showing data that is within the theoretical range. Turbulent measurements have a slightly higher variation but overall there is also a good agreement to the reference measurement, showing that no significant change in data quality is introduced.

In Fig. 8(b), the Hydromast HM200 data is shown for V_f. The measurements agree well with the ADV within the estimated measurement range. Above 0.6 m/s, dominant frequencies are still detected but seem to drift away from the reference value. This change is probably due to a mode shift in vibration occurring near $V_r = 15$. It was seen that above this value also tilt does not change anymore, the vibration is somewhat altered and does not represent velocity changes well, even though peaks in the energy spectrum are still present. As there was no good indicator found in the spectra to filter the "out-of-range" data, V_θ could be used as an indicator of the velocity range so that if V_θ is out of its measurement range, no output of V_f is provided. Points with this criterion applied are indicated in Fig. 8(b) as empty symbols. For all the data, the RMSE value is 0.113 m/s, whereas the data with V_θ-based criteria (filled symbols) has RMSE 0.03 m/s. Alternatively, an empirical calibration fit could be used on the data, which follows the higher-end frequencies better and accounts for that mode change. But with this approach, there is the downside that each membrane needs an extended calibration in similar flow conditions as the application.

Tilt-based velocities from HM300 are shown in Fig. 9(a). Below 0.15 m/s, which is the lower theoretical measurement limit, the measurements have a constant value and are not usable (empty symbols indicate "out-of-range" data). There is an agreement between ADV and Hydromast from 0.15 m/s up to even 1.0 m/s, with RMSE of 0.047 m/s excluding turbulent and out of range points (RMSE is 0.093 m/s including all points). The measurement range is higher than the one achieved in calibration but seems that the lower sensitivity to flow velocity (as discussed above in Section III) allows a much wider measurement range. This demonstrates that the HM300 can be used on its own for a wide range of velocity measurements from 0.1 to 1.0 m/s, compared to V_f measurement range being only one-third of it. Only some of the high turbulence data at higher velocities is not following the trend, therefore care needs to be taken at very turbulent conditions at high flow speeds (higher than V_f range).

Fig. 9(b) shows results for tilt-based V_θ for HM200. At low velocities, the "out-of-range" data is again constant as for the other mast (hollow symbols). Above that, there is an excellent agreement between ADV and Hydromast measurements between 0.3 m/s and 0.7 m/s, where in-range data is marked with filled symbols and having RMSE of 0.03 m/s. Above that, the HM200 has reached its maximum tilt angle and does not capture flow velocities above 0.7 m/s. Out-of-range data based on magnitude limits is shown with empty symbols and it can be seen that this criterion works well for these velocities, filtering out data that does not represent correct velocities. For HM200, the working range of V_θ is the same as the theoretical range of V_f in Table I.

Overall, both velocity estimates agree well with the reference measurements. Some of the highly turbulent data do not follow general trends, but there seems not to be any systematic impact. In high turbulence conditions and high speeds, the data has lower accuracy and could overestimate the flow speed, whereas at lower speeds high TI does not seem to affect the results.

A set of measurements were also performed to evaluate the flow direction. For direction, no calibration is needed, as the direction $\bar{\phi}$ can be calculated directly from the Hall sensor output. For this, the full experimental setup was rotated by 45° increments, and measurements from Hydromast and ADV were compared. This was done with both devices, at several flow speeds, to test the sensitivity at slow, medium, and high velocities. The measured angles compared with the ADV reference are shown in Fig. 10. Both Hydromasts show a very good direction estimate, having RMSE of 3.46°. The variation is bigger in places where also ADV had higher RMSE, showing that there was higher variability in flow, resulting in less reliable results.

B. Steady Flow, Long-Term Tests

A long-term river test was performed to verify the Hydromast durability and performance, as well as demonstrate the near real-time flow monitoring. Two devices were deployed, in the same configuration as shown in Fig. 7. Validation measurements were taken with an ADV (Vectrino Profiler, Nortek AS, Norway) every second day over a two-week testing period. The validation test was carried out in Vääna river (latitude: 59.292888 N, longitude 24.739287 E; closest address Otto tee, Lokuti, 75 514 Harjumaa, Estonia).

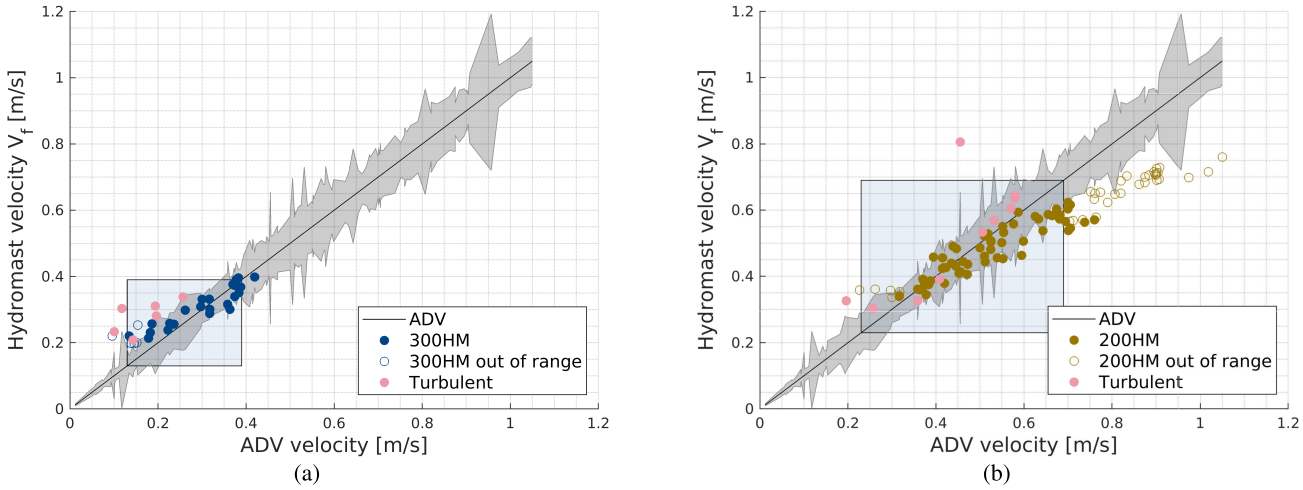

Fig. 8. Steady flow short-term validation data for frequency-based velocity estimate V_f. (a) 300-mm mast and (b) 200-mm mast. Filled symbols denote the data in range and empty symbols out of range. SD ranges from ADV measurements are shaded in gray. The blue box indicates the theoretical measurement range.

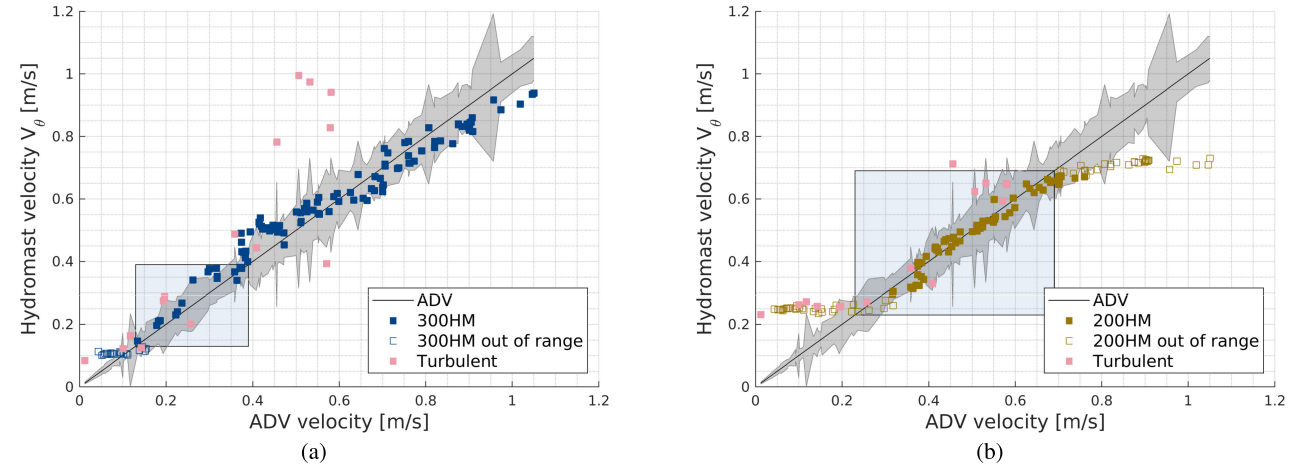

Fig. 9. Steady flow short-term validation data for tilt-based velocity estimate V_θ (a) 300-mm mast and (b) 200-mm mast. Filled symbols denote the data in range and empty symbols out of range. SD ranges from ADV measurements are shaded in gray. The blue box indicates the theoretical measurement range.

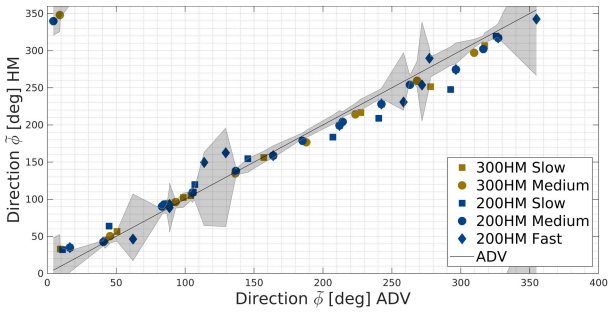

Fig. 10. Flow direction $\bar{\phi}$ validation data. The direction measurements were done in varying flow conditions slow (up to 0.22 m/s), medium (up to 0.61 m/s), and fast (up to 0.85 m/s).

In this experimental setup, the devices were streaming data online with the framework described in Section II-C. The two Hydromasts were connected to a Raspberry Pi 3 (Raspberry Pi Foundation in association with Broadcom) microcomputer running Balena OS, which was battery and solar panel-powered over the whole testing period. The live data stream monitoring over the GSM network allowed us to evaluate the Hydromast performance as well as detect faults in the measurements. This allowed near real-time monitoring (about 3 s latency) of river flow velocity, water level, and also direction.

The average velocities throughout the two-week tests for both HM200 and HM300 are shown in Fig. 11(a). The frequency-based velocity V_f was estimated for 30-s intervals and averaged over 30-min periods. The tilt-based V_θ has been calculated as instantaneous velocity and averaged over 30-min periods. These tests were run during spring entering into the dry season, hence, the river water flow velocity decreases over time. Both V_θ and V_f show a steady decrease in flow velocity from 0.37 to 0.2 m/s and agree well with the ADV reference measurements taken. For tilt-based V_θ from HM300, higher variations in speed are captured compared to V_f. For higher speeds during the first days, V_θ seems to overestimate compared to the reference velocities, but both measurements are within the ADV SD range. After the 4th of April, when speeds are lower, the agreement with ADV

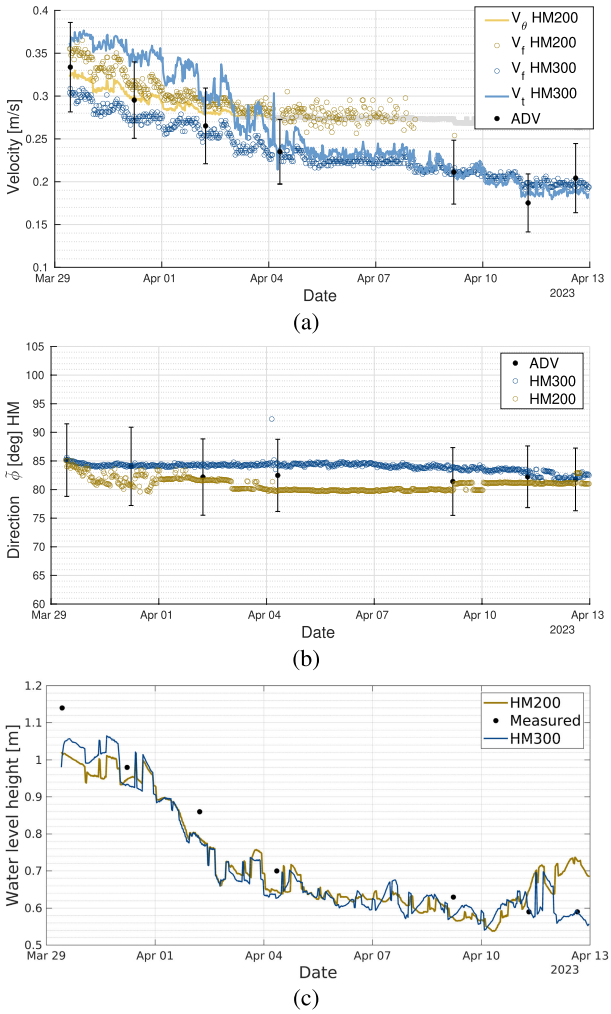

Fig. 11. Steady flow long-term validation data in Vääna river. Results averaged over 30 min. (a) Frequency and tilt-based velocity estimates. (b) Flow direction ϕ. (c) Water level height.

reference measurements becomes very good for both of the velocity estimates.

As for HM200, V_θ and V_f measure continuously during the first days and agree very well with each other and with reference ADV measurements. After 4th April 2023 flow velocity started to fall below the measurement range of the HM200 and it does not give an accurate estimate anymore. For V_θ, M_{XYZ} goes below the minimum limit defined earlier (data marked as light gray) and for V_f, fewer high-energy peaks are detected.

In addition, flow direction was estimated for the same experiments, and the results are shown together with the ADV direction in Fig. 11(b). As there was no specific device orientation reference taken at the test site, a comparison with ADV was made using the first measurement point. Based on that, a constant offset of 5° was removed from the Hydromast data.

In Fig. 11(c), the water level height estimates using the Hydromast are shown. Tallinn-Harku weather station data [33] was used as the atmospheric pressure reference and manual measurements were taken for comparison during ADV measurements. Both Hydromasts behave similarly well and agree

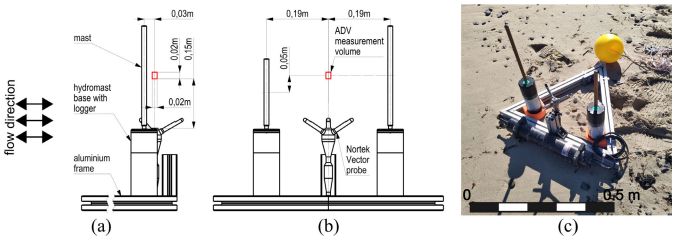

Fig. 12. Setup for unsteady flow validation tests in the sea. (a) Side view and (b) front view with the ADV and Hydromast placement. (c) Assembled setup in the field.

with the measurement points, all estimates varying within the 10-cm range. HM200 does not follow the trend during the last two days and this is due to a failure of the pressure sensor, which was determined after the tests.

C. Unsteady Flow

Several tests were conducted in the sea, near the coast, to validate the behavior of the Hydromast in unsteady waves with varying flow direction and magnitude. Measurements were done for 10-min time periods, to allow long enough datasets for spectral analysis with an acquisition rate of 50 Hz. A commercial ADV (Vector, Nortek AS, Norway) was used as the reference measurement device, with an acquisition rate of 8 Hz. Two Hydromasts, HM200 and HM300, together with the ADV probe in between were installed on a solid frame and immersed in the sea on a sandy flat surface, at about 0.9-m depth. The experimental setup of this test is shown in Fig. 12.

To validate the unsteady velocity estimations, measurements were taken simultaneously for the two Hydromasts and ADV. The experiments were done on two days: on 4th May 2023 in Pikakari beach (lat: 59°28'26.2"N long: 24°43'27.4"E) and on 18th May 2023 at Vääna beach (lat:59°25'29.0"N long: 24°20'19.1"E). Locations and days were chosen to test devices at different flow conditions. For both, the Hydromast and the ADV, the first velocity estimations were done on raw data. The resulting velocity estimations were then passed through a low-pass filter with cutoff frequency 2 Hz for consistency and better comparison.

On the 4th of May, the conditions were very calm, the maximum velocity reached was 0.3 m/s. These velocities were below the HM200 measurement range, and therefore only HM300 data is analyzed and shown. Fig. 13 shows 5 min of the measurements of ADV and HM300. It can be seen that the Hydromast shows similar behavior in velocity magnitude as the reference ADV. It can clearly be seen that HM300 follows nicely the same trend as the reference measurement for higher flow speeds, demonstrating the capability of the Hydromast to estimate instantaneous flow velocities in unsteady flow.

The unsteady measurements on 18th May 2023 are shown in Fig. 14(a) and (b), for HM300 and HM200, respectively. In this case, the velocity was within the measurement range for both devices. HM300 shows a very good correlation throughout the data, following all the ADV peaks closely, especially well seen at the zoom-in. HM200 in Fig. 14(b) shows agreement with ADV at higher speeds but is cutting off the lower velocities, as it is not sensitive enough at low speeds. At speeds above the minimum theoretical range,

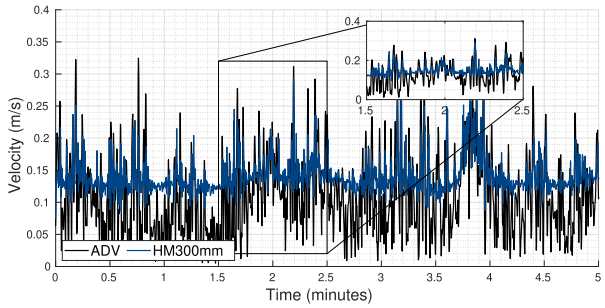

Fig. 13. Unsteady flow tilt-based velocity validation test Pikakari beach, 4 May 2023, 300-mm mast.

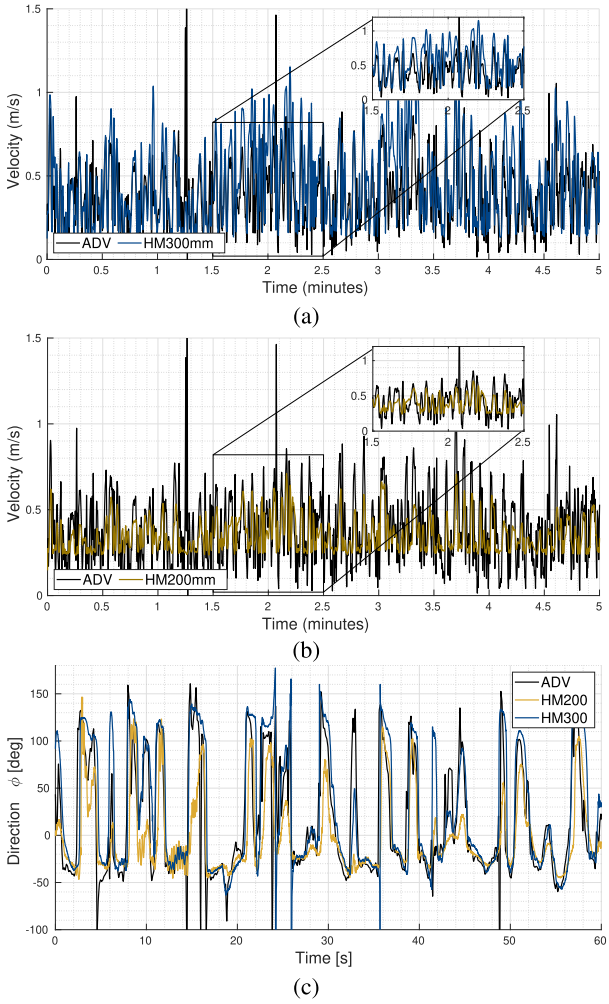

Fig. 14. Unsteady flow validation tests, Vääna beach, 18th May 2023. (a) Tilt-based velocity, 300-mm mast. (b) Tilt-based velocity, 200-mm mast. (c) Direction ϕ, 200- and 300-mm mast.

a very good correlation with the reference measurement can be observed. The root-mean-square deviation from ADV data was 0.095 m/s for HM200 and 0.101 m/s for HM300.

In addition, both HM200 and HM300 were used to estimate the flow directions during the 18th May experiments when the flow speed was high enough to work with both masts. A short 1-min segment of the directions is shown in Fig. 14(c). The direction varies a lot as the flow near the coast has short waves due to wind and swell. Direction estimations from both devices show very good agreement when compared to the ADV, having an equally fast reaction to the change of direction.

V. Discussion

The characterization and validation of the Hydromast with the Hall effect sensor have been performed. Both velocity estimates, the frequency-based velocity V_f and the tilt-based V_θ perform well in measuring flow velocities in various setups. For V_f, the functional dependency as well as the working range agree well with the described theoretical framework. Furthermore, the longer mast HM300 resolves well lower velocities and can be easily used as an independent measurement. For the shorter mast HM200, the velocity range is wider, but an extra range criteria based on V_θ needs to be used to detect the measurement range and allow accurate velocity estimates. However, HM200 measurements are more robust, whereas overlap for HM300 is relatively small for V_f and V_θ.

When calculating average flow speeds over longer periods of time using HM200, care needs to be taken to interpret the low-velocity data. Around the lower limit of the measurement range frequency-based estimations only occur for higher velocities for HM200 and not for lower, which can lead to biased results. One option would be using an estimate from tilt as an indicator if V_f is reliable, similar to what was suggested for upper velocities in the short validation tests. Furthermore, a minimum number of samples required for the average can be implemented.

As for the tilt-based V_θ, for HM300, the measurement range is three times larger than for V_f, allowing the device to be used in applications with high velocity variations. For HM200, the range is comparable with V_f, giving independent and reliable velocity estimates. Using V_θ, instantaneous velocities in changing flow conditions can be measured, allowing measurements in areas where flow direction is constantly changing, like with the waves on the coast. Here again, HM300 seems to perform better, capturing lower velocities than HM200 and both sensors seem to capture higher velocities.

In unsteady flow, the ADV velocity and the Hydromast velocity showed a good correlation. However, the measurements were taken in not ideal conditions for the ADV, namely the experiments were done in shallow water (i.e., ADV was both close to the bottom and near the surface). For more robust unsteady flow characterization, additional work is needed to accurately describe the Hydromast reaction time for instantaneous measurements.

Direction estimate and water column height measurements were done against reference measurements in different flows. The estimates agreed between devices as well as with the references show that they are reliable extra measurements that can be taken during testing. In steady river flow, there was very little variation and the results just show the stability of the direction measurement in time, which agrees with ADV estimates within 5°. The Hydromast has the capability of near real-time data monitoring when a sensor hub can be mounted above water. This is useful for long-term measurements and is also helpful for fault detection.

Based on the validation data, the overall uncertainties of the measurements were estimated for the 95% confidence

TABLE II
UNCERTAINTY ESTIMATES (95% CONFIDENCE LEVEL)

Mast	V_f [m/s]	V_θ [m/s]	$\bar{\phi}$ [deg]	Water level [m]
HM200	0.096	0.050	12.10	0.004
HM300	0.049	0.094	12.02	0.003
ADV	0.129	0.129	36.45	N/A

level, reported in Table II. The same estimates for ADV have also been shown for comparison. As both velocity estimates have their own pros and cons, it could be considered to use the two independent velocity estimates in parallel and combine them for higher accuracy. Alternatively, for higher accuracy, calibrations can be performed before the actual tests in similar flow conditions to capture the specific behavior. High turbulence levels would provide rapid changes in velocity output and that could be an indicator that caution needs to be taken in data interpretation.

The Hydromast measurements are independent of the water quality and surface reflections, allowing it to be used also in locations, where acoustic methods fail. In the future, more reliable pressure sensors should be used to avoid drifting and provide more reliable water level height data. Additional research could be done on fault detection and unwanted debris detection. Also, finding a way to estimate TI from the Hydromast output would be a useful feature, to indicate high turbulence conditions.

The compact design and affordable price of the Hydromast (roughly 1/10th of a commercial ADV) coupled with its versatile communication capabilities, make it suitable for a wide range of applications in shallow water environments. Its low cost enables distributed sensing in various applications, including improving safety in harbors by monitoring currents, detecting ship traffic along coastlines, and evaluating bed load for sediment transportation studies. Furthermore, the distributed sensing capability allows for the application of these devices in the aquaculture industry, as well as in the field of renewable energy, for site monitoring and site evaluation.

VI. CONCLUSION

In this article, the Hall effect sensor-based low-cost flow monitoring device Hydromast has been introduced. The device was characterized and validated against a commercial ADV and shown to perform well in various flows, with flow speeds from 0.15 to 1 m/s. With this new device, average and instantaneous flow speed along with flow direction and water depth can be measured, allowing the devices to be used in both steady and fluctuating flow conditions. Cloud communication functionalities were developed so that monitoring can be done online, allowing long-term testing with live outputs and data analysis, as well as allowing fault detection. With low cost and high reliability in near-bed flow estimations, the described device can be used in various flow conditions for flow velocity and direction estimation, both short- and long-term flow monitoring, as a single device or in a larger grid with near real-time data output to the user.

ACKNOWLEDGMENT

The authors would like to thank Jaan Rebane and Andres Ernits for their support with Hydromast Manufacturing and Prof. Jeffrey Andrew Tuhtan for the fruitful discussions.

REFERENCES

[1] S. Dingman, *Physical Hydrology*. Long Grove, IL, USA: Waveland Press, 2015.
[2] A. J. Kalmijn, "Hydrodynamic and acoustic field detection," in *Sensory Biology of Aquatic Animals*. New York, NY, USA: Springer, 1988, pp. 83–130.
[3] K. F. E. Betteridge, J. J. Williams, P. D. Thorne, and P. S. Bell, "Acoustic instrumentation for measuring near-bed sediment processes and hydrodynamics," *J. Experim. Mar. Biol. Ecol.*, vols. 285–286, pp. 105–118, Feb. 2003.
[4] R. Kostaschuk, J. Best, P. Villard, J. Peakall, and M. Franklin, "Measuring flow velocity and sediment transport with an acoustic Doppler current profiler," *Geomorphology*, vol. 68, nos. 1–2, pp. 25–37, May 2005.
[5] B. Elfrink and T. Baldock, "Hydrodynamics and sediment transport in the swash zone: A review and perspectives," *Coastal Eng.*, vol. 45, nos. 3–4, pp. 149–167, May 2002.
[6] F. D. Shields and J. R. Rigby, "River habitat quality from river velocities measured using acoustic Doppler current profiler," *Environ. Manage.*, vol. 36, no. 4, pp. 565–575, Oct. 2005.
[7] L. A. Levin et al., "The function of marine critical transition zones and the importance of sediment biodiversity," *Ecosystems*, vol. 4, no. 5, pp. 430–451, Aug. 2001.
[8] W. Wu, R. Emerton, Q. Duan, A. W. Wood, F. Wetterhall, and D. E. Robertson, "Ensemble flood forecasting: Current status and future opportunities," *Wiley Interdiscipl. Rev., Water*, vol. 7, no. 3, p. e1432, May 2020.
[9] A. Recking, "Theoretical development on the effects of changing flow hydraulics on incipient bed load motion," *Water Resour. Res.*, vol. 45, no. 4, pp. 1–16, Apr. 2009, doi: 10.1029/2008WR006826.
[10] B. N. Bockelmann, E. K. Fenrich, B. Lin, and R. A. Falconer, "Development of an ecohydraulics model for stream and river restoration," *Ecol. Eng.*, vol. 22, nos. 4–5, pp. 227–235, Jul. 2004.
[11] C. Tomsett and J. Leyland, "Remote sensing of river corridors: A review of current trends and future directions," *River Res. Appl.*, vol. 35, no. 7, pp. 779–803, Sep. 2019.
[12] G. Dolcetti, B. Hortobágyi, M. Perks, S. J. Tait, and N. Dervilis, "Using noncontact measurement of water surface dynamics to estimate river discharge," *Water Resour. Res.*, vol. 58, no. 9, Sep. 2022, Art. no. e2022WR032829.
[13] Planet Inc. SkySat. *Planet Developers*. Accessed: Jul. 17, 2023. [Online]. Available: https://developers.planet.com/docs/data/skysat/
[14] SkySat. *European Space Agency*. Accessed: Jul. 17, 2023. [Online]. Available: https://earth.esa.int/eogateway/missions/skysat#instruments-section
[15] M. C. Stone and R. H. Hotchkiss, "Evaluating velocity measurement techniques in shallow streams," *J. Hydraulic Res.*, vol. 45, no. 6, pp. 752–762, Nov. 2007.
[16] W. J. Plant, W. C. Keller, and K. Hayes, "Measurement of river surface currents with coherent microwave systems," *IEEE Trans. Geosci. Remote Sens.*, vol. 43, no. 6, pp. 1242–1257, Jun. 2005.
[17] R. P. Mied et al., "Airborne remote sensing of surface velocities in a tidal river," *IEEE Trans. Geosci. Remote Sens.*, vol. 56, no. 8, pp. 4559–4567, Aug. 2018.
[18] A. Hauet, J.-D. Creutin, and P. Belleudy, "Sensitivity study of large-scale particle image velocimetry measurement of river discharge using numerical simulation," *J. Hydrol.*, vol. 349, nos. 1–2, pp. 178–190, Jan. 2008.
[19] M. Marian, J. Kim, and D. Kim, "Impact of the sampling duration on the uncertainty of averaged velocity measurements with acoustic instruments," *Hydrolog. Processes*, vol. 35, no. 4, Apr. 2021, Art. no. e14125. [Online]. Available: https://doi.org/10.1002/hyp.14125
[20] U. C. E. Zanke, "On the influence of turbulence on the initiation of sediment motion," *Int. J. Sediment Res.*, vol. 18, no. 1, pp. 17–31, Jan. 2003.
[21] E. Muller, H. Décamps, and M. K. Dobson, "Contribution of space remote sensing to river studies," *Freshwater Biol.*, vol. 29, no. 2, pp. 301–312, Apr. 1993.

[22] M. Rätsep, K. E. Parnell, T. Soomere, M. Kruusmaa, A. Ristolainen, and J. A. Tuhtan, "Surface vessel localization from wake measurements using an array of pressure sensors in the littoral zone," *Ocean Eng.*, vol. 233, Aug. 2021, Art. no. 109156.

[23] P. Wang, X. Tian, T. Peng, and Y. Luo, "A review of the state-of-the-art developments in the field monitoring of offshore structures," *Ocean Eng.*, vol. 147, pp. 148–164, Jan. 2018.

[24] A. Ristolainen, J. A. Tuhtan, A. Kuusik, and M. Kruusmaa, "Hydromast: A bioinspired flow sensor with accelerometers," in *Biomimetic and Biohybrid Systems*, vol. 9793, N. F. Lepora, A. Mura, H. G. Krapp, P. F. M. J. Verschure, and T. J. Prescott, Eds. Berlin, Germany: Springer, 2016, pp. 510–517.

[25] A. Ristolainen, K. Kalev, J. A. Tuhtan, A. Kuusik, and M. Kruusmaa, "Hydromorphological classification using synchronous pressure and inertial sensing," *IEEE Trans. Geosci. Remote Sens.*, vol. 56, no. 6, pp. 3222–3232, Jun. 2018.

[26] A. Ristolainen, J. A. Tuhtan, and M. Kruusmaa, "Continuous, near-bed current velocity estimation using pressure and inertial sensing," *IEEE Sensors J.*, vol. 19, no. 24, pp. 12398–12406, Dec. 2019.

[27] E. Naudascher and D. Rockwell, *Flow-Induced Vibrations: An Engineering Guide*. New York, NY, USA: Dover, 2005.

[28] F. M. White, *Viscous Fluid Flow*, 3rd ed. New York, NY, USA: McGraw-Hill, 2006.

[29] G. Voulgaris and J. H. Trowbridge, "Evaluation of the acoustic Doppler velocimeter (ADV) for turbulence measurements," *J. Atmos. Ocean. Technol.*, vol. 15, no. 1, pp. 272–289, Feb. 1998.

[30] L. Vihman and J. Raik, "Adaptive Kalman filter based data aggregation in fault-resilient underwater sensor networks," in *Proc. 24th Int. Conf. Digit. Signal Process.*, Jun. 2023, pp. 1–5.

[31] L. Vihman, M. Kruusmaa, and J. Raik, "Data-driven cross-layer fault management architecture for sensor networks," in *Proc. 16th Eur. Dependable Comput. Conf. (EDCC)*, Munich, Germany, Sep. 2020, pp. 33–40, doi: 10.1109/EDCC51268.2020.00015.

[32] Keskonnaagentuur. (2023). *Vaatlusandmed*. Keila River Water Station. Accessed: Jun. 20, 2023. [Online]. Available: https: www.ilmateenistus.ee/siseveed/vaatlusandmed/tabel

[33] Keskonnaagentuur. 2023. *Vaatlusandmed*. Tallinn-Harku Weather Station. Accessed: Jun. 20, 2023. [Online]. Available: https:www.ilmateenistus.ee/ilm/ilmavaatlused/vaatlusandmed/tunniandmed

Margit Egerer received the B.Sc. degree in engineering physics from the Tallinn University of Technology, Tallinn, Estonia, in 2007, the M.Sc. degree in mechanics of solids and fluids from Chalmers University, Göteborg, Sweden, in 2010, and the M.A. and Ph.D. degrees in mechanical and aerospace engineering from Princeton University, Princeton, NJ, USA, in 2012 and 2014, respectively.

She is currently a Researcher with the Center for Biorobotics, School of Information Technologies, Tallinn University of Technology. Her research interests include fluid flow sensors, environmental sensing, and experimental fluid dynamics.

Asko Ristolainen received the B.Sc. and M.Sc. degrees in mechatronics and the Ph.D. degree in information and communication technology from the Tallinn University of Technology, Tallinn, Estonia, in 2008, 2010, and 2015, respectively.

He is currently a Senior Researcher with the Center for Biorobotics, School of Information Technologies, Tallinn University of Technology, where he is involved in the H2020 ILIAD Project. His research interests include tactile and flow sensor design in robotics and remote environmental sensing.

Laura Piho received the M.Sc. degree in mathematics from the University of Leicester, Leicester, U.K., in 2015, and the Ph.D. degree in engineering from the University of Warwick, Coventry, U.K., in 2019.

She is currently a Researcher with the Center for Biorobotics, Tallinn University of Technology, Tallinn, Estonia. During the past years, she has been involved in data analysis and processing for flow sensing and bio-inspired robot locomotion. Her research mainly focuses on signal processing, time-series analysis, and statistical modeling for bio-inspired robotics and environmental sensing.

Lauri Vihman received the B.Sc. and M.Sc. degrees in computer science from the Tallinn University of Technology, Tallinn, Estonia, in 2013 and 2016, respectively.

He is currently an Early Stage Researcher with the Center for Dependable Computing Systems, Tallinn University of Technology. His research focuses on cross-layer reliability in sensor networks.

Maarja Kruusmaa received the Ph.D. degree from the Chalmers University of Technology, Göteborg, Sweden, in 2002.

Since 2008, she has been a Professor with the Tallinn University of Technology (TalTech), Tallinn, Estonia, as a PI of the Center for Biororobitcs, a research group focusing on bio-inspired robotics, underwater robotics, and novel underwater sensing technologies. From 2017 to 2022, she was a Visiting Professor at the Center for Excellence of Autonomous Marine Operations and Systems (NTNU AMOS). Her research interests include novel locomotion mechanisms for underwater environments on flowable media and novel methods for underwater flow sensing.